DOI: 10.1002/((please add manuscript number))
Article type: Communication

Band gap Tunability in Sb-alloyed $BiVO_4$ Quaternary Oxides as Visible-Light Absorbers for Solar Fuel Applications

*Anna Loiudice, Jie Ma, Walter S. Drisdell, Tracy M. Mattox, Timothy Thao, Jason K. Cooper, Cinzia Giannini, Junko Yano, Ian D. Sharp, Lin-Wang Wang, and Raffaella Buonsanti**

Dr. A. Loiudice, Dr. J. Ma, Dr. W. S. Drisdell, T. Thao, Dr. J. K. Cooper, Dr. J. Yano, Dr. I. D. Sharp, Dr. L.-W. Wang, Dr. R. Buonsanti
Joint Center for Artificial Photosynthesis, Lawrence Berkeley National Laboratory, Berkeley, California 94720, United States.
Dr. A. Loiudice, Dr. J. Ma, Dr. W. Drisdell, Dr. J. K. Cooper, Dr. J. Yano, Dr. L.-W. Wang, Dr. R. Buonsanti
Materials Sciences Division, Lawrence Berkeley National Laboratory, One Cyclotron Road, Berkeley, CA 94720, United States.
T. M. Mattox
The Molecular Foundry, Lawrence Berkeley National Laboratory, One Cyclotron Road, Berkeley, CA 94720, United States.
Dr. I. D. Sharp
Physical Biosciences Division, Lawrence Berkeley National Laboratory, One Cyclotron Road, Berkeley, CA 94720, United States.
Dr. C. Giannini
Institute of Crystallography, National Research Council, v. Amendola 122/O, Bari, 70126, Italy

E-mail: rbuonsanti@lbl.gov
Dr. R. Buonsanti
Joint Center for Artificial Photosynthesis, Lawrence Berkeley National Laboratory, Berkeley, California 94720, United States.
Materials Sciences Division, Lawrence Berkeley National Laboratory, One Cyclotron Road, Berkeley, CA 94720, United States.

Keywords: (quaternary oxides, solar energy conversion, light absorbers, colloidal synthesis, materials discovery)

Storage of intermittent renewable energy is emerging as a critical need to reduce the global dependence on fossil fuels and to move towards a more sustainable society. Solar-to-chemical energy conversion is a promising approach for addressing this challenge and is at the forefront of materials research in this area. To efficiently generate carbon-neutral fuels from sunlight, water, and CO_2, individual light absorbing materials that meet the following criteria must be

identified: i) band gap in the range of 1.7-2.2 eV to absorb a large fraction of the solar spectrum; ii) band edge positions suitable to reduce CO_2 (or H_2O) and to oxidize H_2O; iii) resistance to photocorrosion.[1,2] Due to the substantial challenge associated with finding a single material possessing all of these properties, tandem light absorber designs have shown the highest photoelectrochemical performance for integrated solar fuels generators.[1,2] In such a tandem architecture, a p-type semiconductor (photocathode) and an n-type semiconductor (photoanode) are utilized to drive the reduction and oxidation half-reactions, respectively.[1,2] While a few strong candidates for photocathodes already exist (i.e. Si, InP), highly efficient photoanode materials have yet to be discovered.[3,4]

The main challenge results from the fact that classical semiconductors used in photovoltaics such as III-V, II-VI, and n-Si, rapidly photo-corrode under the harsh oxidizing conditions required for water splitting.[5] Although there have been considerable advances in the development of protection layers for stabilization of otherwise unstable photoanodes, there remains a pressing need for discovery of intrinsically stable materials to provide a path to large area, low cost, and durable devices that can make a practical impact on energy conversion technologies.[6-8] Oxide semiconductors have significant potential due to their improved resistance to photocorrosion relative to other semiconductors. However, most of the binary metal oxides (i.e. TiO_2, WO_3, ZnO) possess wide band gaps and their optical absorption is limited to the blue and UV portion of the solar spectrum.[9-23] For a tandem architecture, the ideal band gap of the top light absorber is ~1.75 eV if combined with n-Si (E_g = 1.1 eV) and NiMo and $NiFeO_x$ earth abundant catalysts.[24] One approach to reducing the band gap is utilization of ternary and quaternary oxides which have been receiving increased attention as light absorbers which, critically, also supply the potential needed to drive multi-electron oxidation reactions.[9-23] In this work, we report the discovery of antimony-alloyed bismuth vanadate (Sb-$BiVO_4$). Through a combination of theoretical predication and experimental validation, we show that this novel photoanode material possesses a band gap

that linearly decreases below 2.4 eV with increasing Sb content. This work is enabled by the development of a novel two-step synthesis process that will broadly aid new materials discovery by providing synthetic access to a wide range of compositionally complex oxides.

Monoclinic bismuth vanadate ($BiVO_4$), with its 2.4-2.5 eV band gap and favourable band alignment for oxygen evolution, is one example of a ternary oxide that has attracted considerable attention as a photoanode for solar fuel applications.[10-18] While $BiVO_4$ has served as a useful material platform to study the complex phenomena emerging in multi-cation oxide light absorbers and significant advances in photocatalytic performance have been realized by controlled doping and mesostructuring, its band gap places fundamental limits of solar energy conversion efficiency below 10%.[24] Therefore, it is necessary to identify oxide light absorbers with smaller and, ideally, controllable band gaps in order to make a practically efficient integrated water splitting device.

$BiVO_4$ is characterized by a layered structure containing cations with formal oxidation states of Bi^{3+} ($6s^2$) and V^{5+} ($3d^0$), in coordination with O^{2-} ($2p^6$) anions. As previously demonstrated, O 2p states contribute to both the valence and conduction band densities of states due to hybridization with Bi 6s and V 3d orbitals, respectively.[15,16] Although Sb-$BiVO_4$ has never been experimentally synthesized, molecular orbital theory suggests that alloying of Sb into $BiVO_4$ has potential to either decrease or increase the band gap, depending on the preferred substitutional site and energetically favoured crystal structure. In particular, when Sb atoms are introduced into the $BiVO_4$ lattice, they could either occupy the Bi sites in a 3+ charge state ($4d^{10}5s^2$), forming $Bi_{1-x}Sb_xVO_4$, or occupy the V sites in a 5+ charge state ($4d^{10}$), thus forming $BiV_{1-x}Sb_xO_4$.

If Sb substitutes on the Bi site and the monoclinic structure is retained, the valence band energy should be raised without significantly affecting the conduction band edge (the vacant Sb 5p orbitals contribute to states well above the conduction band minimum (CBM)), thus reducing the final band gap. This is because the occupied 5s level of Sb is energetically higher

than the 6s level of Bi; the ionization potential of Sb^{3+} is 44.2 eV while it is 45.3 eV for Bi^{3+}.[25] Therefore, valence band lifting is expected based on a stronger 5s-2p coupling between Sb and O. On the other hand, if Sb substitutes V the valence of Sb is expected to be $4d^{10}$ and the CBM is dominated by hybridized Sb 4s and V 3d orbitals. As such, the conduction band should lift and the band gap increase with the Sb content because the Sb 4s orbitals are higher in energy than the V 3d orbitals.[25]

From an experimental standpoint, the synthetic challenge associated with accessing multi-component materials, such as Sb-$BiVO_4$, with systematic and precise definition of composition and microstructure is significant; it relies on establishing control over the reactivities of three or more metal precursors and on identifying the conditions required to form compositions and structures with desired function. Hence, devising robust synthetic approaches to complex materials is essential for validating theoretical predictions and providing a foundation for discovery science. Herein, a novel two-step synthetic strategy is designed for precisely tuning the composition and retaining the monoclinic structure of Sb-$BiVO_4$ films over a wide compositional range. $Bi_{1-x}Sb_x$ colloidal nanocrystals (NCs), with variable composition, *x*, are used as seeds for the growth of the Sb-$BiVO_4$ through chemical and thermal treatments (**Scheme 1**). X-ray absorption confirms that Sb is in a +5 oxidation state and supports the substitution of the V site. A complete structural and optical characterization of the synthesized materials reveals that the monoclinic phase is maintained but a linear band gap reduction with increasing Sb content is observed, contrary to our expectations. First-principles calculations indicates the $BiV_{1-x}Sb_xO_4$ alloy to be the stable phase and provides the insight into the band structure of the alloy and an understanding of the reduced band gap. Finally, the generality of the proposed synthetic strategy to access different ternary oxide light absorbers, and thus aid in future material discovery efforts, is demonstrated.

In the first step, $Bi_{1-x}Sb_x$ NC alloys with different compositions ($0 < x < 1$) were synthetized by following a procedure reported by Zhang et al.[26] Figure S1a shows a transmission electron microscopy (TEM) image of $Bi_{1-x}Sb_x$ NCs, which are characterized by uniform, nearly spherical particles with an average size of 9 nm. As shown in the powder X-ray diffraction (XRD) patterns in Figure S1b, the diffraction peaks of the rhombohedral lattice progressively shifted to higher 2Theta angles with increasing Sb content due to the lattice constant reduction associated with replacement of larger Bi atoms by smaller Sb atoms.[26] The Bi and Sb contents were determined by inductively coupled plasma optical emission spectroscopy (ICP-OES) analysis (Table S1).

To convert the $Bi_{1-x}Sb_x$ seeds into Sb-$BiVO_4$ films, the $Bi_{1-x}Sb_x$ NCs were deposited onto the desired substrate by drop casting and the surface was then fully covered by 100 μl of 150 mM of $VO(acac)_2$ in a dimethyl sulfoxide solution. The film was then annealed at 450 ºC for 2 h in air. During the heating procedure, $Bi_{1-x}Sb_x$ NCs were oxidized and reacted with $VO(acac)_2$ to form Sb-$BiVO_4$. Excess vanadium precursor was used to ensure the complete conversion of the $Bi_{1-x}Sb_x$ seeds to Sb-$BiVO_4$. Residual V_2O_5 formed during the process was removed by soaking the film in a 1 M NaOH solution for 30 s. This process resulted in highly porous films, as shown by scanning electron microscopy (Figure S2). ICP-OES was employed to assess the composition of the synthetized Sb-$BiVO_4$ films (Table S2). Five alloys were produced with Sb content of 2.2%, 7.3%, 12.3%, 20.1% and 25.9%. These Sb percentages are relative to the Bi and V content in the films (Sb+Bi+V=100%). Pure bismuth vanadate and antimony vanadate films were also synthesized from only Bi NCs and only Sb NCs seeds, respectively.

The purity and crystallinity of the Sb-$BiVO_4$ films were confirmed by XRD, as shown in **Figure 1**. Quantitative Rietveld analysis of XRD data confirmed the presence of pure monoclinic phase in the Sb-$BiVO_4$ films up to an Sb content of 20.1%; no evidence of secondary phases such as $BiSbO_4$ or $SbVO_4$ (Figures S3 and S4, Table S3). The refined

structural parameters and the slight shift to higher 2Theta angles of the XRD patterns point to a reduction of the monoclinic $BiVO_4$ unit cell lattice parameters when Sb is present (Table S3). As the Sb content is further increased, two distinct phases, corresponding to monoclinic $BiVO_4$ and rutile $SbVO_4$ phases, are observed. When pure Sb NCs are used as seeds, both $SbVO_4$ and the Sb_2VO_5 phases are observed (Figure S4, Table S3).

The oxidation states of Bi, Sb, and V in the synthetized quaternary oxides were determined by X-Ray photoelectron spectroscopy (XPS) (**Figures 2**a and S5, Table S4). The Bi $4f_{7/2}$ core level spectra were fitted with a peak centered at 159.1 eV, which is consistent with Bi^{3+} (Figure S5). The presence of Bi^0 is not observed in any sample. Analysis of the V $2p_{3/2}$ peak revealed that only one spectral component centered at 516.8 eV fits well all the spectra up to an Sb content of 20%, resulting in an oxidation state of +5. For the case of Sb, identification of the oxidation state is complicated by significant overlap of O 1s and Sb $3d_{5/2}$ core level photoemission lines. The spin orbit split Sb $3d_{3/2}$ component, located at 540.1 eV, is well separated from other spectral features and its intensity increases with Sb content in the Sb-$BiVO_4$ films. In order to quantify the contribution of the individual lines for O 1s and Sb $3d_{5/2}$, XPS spectra of metal Sb, Sb_2O_3 and Sb_2O_5 standards were measured (Figure S5A, Table S4). The peak area ratio of Sb $3d_{5/2}$ and Sb $3d_{3/2}$ in the oxides was 1.56, and this value was used as constrain for fitting XPS spectra. The Sb $3d_{5/2}$ peak position was subsequently found to be at 530.9 eV resulting in a spin orbit splitting of 9.2 eV. While the binding energies from the XPS analysis suggest the presence of Sb 5+ from the comparison with the standards, this statement is still not conclusive due to the uncertainty in the O peaks fitting.

To gain additional information about the oxidation state and local structure of Sb in Sb-$BiVO_4$ thin films, X-ray absorption near edge structure (XANES) and extended x-ray absorption fine structure (EXAFS) measurements were carried out (Figure 2b,c). XANES spectra were collected at the Sb K-edge for the antimony vanadate sample and three Sb-$BiVO_4$ alloys with Sb content of 7.3%, 12.3% and 20.1% (Figure 2b). Comparing the samples to Sb_2O_3 and

Sb_2O_5 standards, the fits of the Sb spectra (data not shown) point at a +5 oxidation state. The EXAFS data are similar for all samples, differing only in the amplitude of the oscillations. The first-shell EXAFS for the Sb-$BiVO_4$ sample with 20.1% of Sb was well described using a theoretical structure in which the Sb substitutes for the V site; the fit is shown in Figure 2c. Fitting parameters are given in the supporting information (Table S5). A reasonable fit could not be achieved for the theoretical structure in which the Sb substitutes for the Bi site. The Sb substituting for the V site is consistent with the findings from both XPS and XANES, which both indicate that Sb is present in the +5 oxidation state. Therefore, we conclude that our synthetic procedure yields monoclinic phase $BiV_{1-x}Sb_xO_4$.

The effect of Sb alloying on the optical properties of the samples were studied by UV-Vis absorption spectroscopy with the samples deposited on quartz glass substrates and the absorption determined by a Kubelka-Munk transformation of the diffuse reflectance spectra, **Figure 3**a. While $BiVO_4$ has been commonly referred to as direct band gap semiconductor, a recent report by Cooper et al. supports the hypothesis that the band gap of monoclinic $BiVO_4$ is indirect with a direct transition present above the minimum indirect transition.[27] Based on this finding, we report the Tauc plots of $BiV_{1-x}Sb_xO_4$ considering both direct and indirect transitions (Figure 3b, c). Linear fitting at the absorption edges, as well as the background due to scattering, of the Tauc plots reveals a reduction of the transition energy with increasing Sb content. Specifically, comparing data from pure $BiVO_4$ to x = 0.2, the indirect band gap decreases from 2.38 eV to 2.28 eV. A reduction in the $(\alpha hv)^2$ plot is also observed which decreases from 2.45 eV to 2.30 eV from x = 0 to x = 0.2 .[27]

As described above, molecular orbital theory would predict that substitutional incorporation of Sb at V sites would increase the band gap relative to pure monoclinic $BiVO_4$. However, optical characterization shows the opposite trend. In order to understand the origin of this unexpected band gap reduction, density functional theory (DFT) calculations of the band structure were performed (see Experimental Section for details). For completeness, two

possible cases for incorporation of Sb atoms in a 5+ oxidation state were considered: $Bi_{1-x}Sb_xVO_4$ and $BiV_{1-x}Sb_xO_4$ alloys. In $Bi_{1-x}Sb_xVO_4$, according to charge neutrality condition, if Sb atom is 5+ charge, then the V atom must be 3+ charge. The calculated energy for the $Bi_{1-x}Sb_xVO_4$ with Sb^{5+} is ~0.14 eV per Sb higher than if Sb were 3+ in this site. Thus, thermodynamics indicates that $BiV_{1-x}Sb_xO_4$ is the most stable phase, in agreement with the conclusion from the experimental results.

For $BiV_{1-x}Sb_xO_4$ alloys, the two pure alloying constituents are $BiVO_4$ and $BiSbO_4$. $BiSbO_4$ and $BiVO_4$ adopt different structures, tetragonal and monoclinic respectively. Because the experimental evidences show that below x = 0.2 the $BiVO_4$ monoclinic structure phase is preserved, the alloying calculations focus on the $BiVO_4$-derived structures. The $BiVO_4$-derived monoclinic structure phase of $BiSbO_4$ is ~ 0.17 eV higher in energy than the ground-state tetragonal structure and exhibits a calculated band gap of ~ 2.3 eV. The calculated band gap for monoclinic $BiVO_4$ is ~ 2.1 eV, consistent with the previous assertion that Sb alloying would increase the band gap if Sb replaces V. The valence band maximum (VBM) of $BiVO_4$ and $BiSbO_4$ are both mainly dominated by the O 2p states.[15,16] However, while the CBM of $BiVO_4$ is mainly constituted by V 3d states, the CBM of $BiSbO_4$ consists primarily of Sb 5s states.

Figure 4a shows the calculated band gap of the $BiV_{1-x}Sb_xO_4$ alloys as a function of x. For traditional alloys, the band gap is expected to transform linearly between the two extremes of x. This is because in traditional alloys the mixing wave functions have the same character (i.e. both s states of Ga and In atoms for the CBM of (Ga,In)P), and the band gap is roughly the compositional-weighted average of the two ending constitutes.[28,29] However, for $BiV_{1-x}Sb_xO_4$ alloys, the band gap almost linearly decreases as the Sb content increases. There are two major factors that affect the band gap in this alloyed system.

First, with Sb incorporation at V the Bi-O bond lengths decrease; consistent with the reduction of the unit cell observed by Rietveld refinement. In $BiVO_4$, the calculated Bi-O

bond lengths are around 2.45 Å, whereas in $BiSbO_4$ they decrease to 2.3 Å. In these materials, Bi atoms are 3+ charged and the Bi s electrons form isolated bands in the lower part of the valence bands. These isolated s bands couple with the O p bands, and raise the energy of the top valence bands. As the Bi-O bond lengths decrease, the s-p coupling is enhanced, and thus the VBM energy increases. The result is a decrease in the band gap. Second, in $BiSbO_4$ the CBM, which is primarily from Sb s, is much higher in energy than that in $BiVO_4$. As such, the calculated band gap is ~ 0.2 eV larger for $BiSbO_4$ than $BiVO_4$. In $BiV_{1-x}Sb_xO_4$ alloys, if the CBM is a mixed state between Sb s and V d bands, the CBM energy should increase with increasing Sb content, in contrast to experimental observations presented above. These two contributions are in opposition for modifying the band gap.

The CBM charge densities in $BiV_{1-x}Sb_xO_4$ alloys with different compositions is shown in Figure 4b. In all these alloys the CBM charge densities are strongly localized at the V atoms (blue spheres), and there is no charge density appearing at the Sb atoms (golden spheres). This observation indicates that in $BiV_{1-x}Sb_xO_4$ alloys, the Sb s states and the V d states do not actually mix. Therefore, in $BiV_{1-x}Sb_xO_4$ alloys the CBM energy is only determined by the V d bands. It is concluded that the second factor, that is the intermixing of Sb s and V d bands in the CBM, does not have a significant contribution to the alloys studied herein and the reduction of the experimentally observed band gap is attributed to a modification of the Bi-O local structure with Sb incorporation.

In summary, the novel two-step NC-seeded growth approach described herein enables access to high surface area, pure phase monoclinic $BiV_{1-x}Sb_xO_4$ films with a tunable Sb content up to $x = 0.2$. Although molecular orbital theory would predict that substitutional incorporation of Sb at V sites should increase the band gap of the alloy, optical characterization reveals a reduced band gap compared to pure monoclinic $BiVO_4$. Furthermore, the band gap linearly decreases with Sb content over the investigated composition range. Comprehensive structural characterization, combined with first-principles calculations, provided insight into the

structure by confirming energetically favourable substitution of V^{5+} by Sb^{5+} in the monoclinic $BiVO_4$ lattice. This substitution results in a decrease of the Bi-O bond length, which is responsible for the band gap reduction. Due to the different character of V d and Sb s states, no orbital mixing occurs which would tend to increase the alloy band gap. The reduced optical band gap is associated with a redshift of the photocurrent onset from incident photon-to-charge conversion efficiency measurements (Figure S6), thereby demonstrating that formation of select quaternary alloys based on the $BiVO_4$ material system has potential for increasing overall solar energy conversion efficiencies. Thus, the results presented here, derived from close coupling of theoretical understanding and advanced synthesis approaches, provide a path to the design of other metal oxides alloys with desirable band gaps and band edge positions for solar water splitting. Indeed, to provide a basis for new materials discovery, as well as to demonstrate the general applicability of the NC-seeded growth approach, other high surface area ternary oxide light absorbers were targeted. Bi_2WO_6, $CuWO_4$, $SnWO_6$, and $InVO_4$ were synthetized and structurally characterized by XRD by using Bi, Cu, Sn and In_2O_3 NC seeds, respectively (**Figure 5**).[20-22] While the exploration of combinations of these, and other materials, is beyond the scope of the present work, because at the present colloidal NCs can be produced with precise tuning in a broad chemical compositional range, this work opens up an almost unlimited access to complex metal oxides with variable composition for a wide range of materials applications.[30,31] While the central focus of the present work has been on synthesis of semiconductor light absorbers, it is important to note that our synthetic approach has potential to enable materials discovery advances in other research fields, such as batteries and fuel cells, that share many of the same challenges relative to the preparation and tunability of multicomponent metal oxides.[32-35] Even more broadly, the present work provides further proof that, to confront the material design challenge and to discover new materials with properties suitable to advance specific applications, the interplay between theoretical predictions and experimental work is crucial.[36-38]

Experimental Section

Experimental Methods: $Bi_{1-x}Sb_x$ seeds were synthesized by following a reported procedure (see Supporting Information for details). The as-prepared seeds were drop cast from hexane on the substrate and covered with100 ml of a 150 μM solution of $VO(acac)_2$ in dimethyl sulfoxide solution. Annealing was carried out at 450ºC for 2 h in air. The excess of V_2O_5 formed during the annealing process was removed by soaking the film in 1M NaOH for 30 s.

Elemental analysis was performed by ICP-OES on a Varian 720 spectrometer on films digested in concentrated HNO_3. The relative error of the extracted Bi, Sb, and V was within 3%, as evaluated on the basis of five replicates per each measurement.

Wide-angle XRD was performed using a Bruker D8-Discover X-ray diffractometer equipped with a GADDS area detector operating at 40 kV and 20 mA with a Cu-Kα source with wavelength of λ = 1.54 Å. Thin films were prepared on silicon substrates. Rietveld analysis was performed by using the whole-profile Rietveld-based fitting approach implemented in the FullProf program (https://www.ill.eu/sites/fullprof/index.html). The analysis allowed the determination of the weight fraction of each crystalline phase in the mixture, along with the unit cell parameters.

XPS was performed using a monochromatized Al Kα source (hν = 1486.6 eV), operated at 225 W, on a Kratos Axis Ultra DLD system at a takeoff angle of 0° relative to the surface normal and a pass energy for narrow scan spectra of 20 eV, corresponding to an instrument resolution of approximately 600 meV. Survey spectra were collected with a pass energy of 80 eV. Spectral fitting was performed using CASA analysis software. Spectral positions were corrected by shifting the primary C 1s core level position to 284.8 eV, and curves were fit with quasi-Voigt lines following Shirley background subtraction. Samples were deposited on conductive silicon substrates for analysis.

UV–Vis diffuse reflectance spectra were recorded on a Shimadzu SolidSpec-3700 spectrometer with a D_2 (deuterium) lamp for the ultraviolet range and a WI (halogen) lamp for

the visible and near-infrared range. Measurements were performed with an integrating sphere. Samples were deposited on quartz substrates for analysis.

XANES and EXAFS spectra were collected at beamline 7-3 at the Stanford Synchrotron Radiation Lightsource (SSRL) at SLAC National Accelerator Laboratory. X-ray radiation was monochromatized using a Si (220) double crystal monochromator. The incident beam intensity was monitored with an Ar-filled ion chamber in front of the sample to correct for any fluctuations. Spectra were collected in fluorescence mode using a 30-element Ge detector (Canberra). Energy was calibrated using an Sb foil. The first peak maximum of the first derivative of the spectrum of the foil (30488.0 eV) was used as a calibration point.

Calculation Methods: Theoretical calculations were based on density functional theory within the generalized gradient approximation formulated by Perdew, Burke and Ernzerhof as implemented in the VASP code.[39-41] The projector augmented wave (PAW) pseudopotentials are employed, and the valence wave functions are expanded in a plane-wave basis with an energy cutoff of 600 eV.[42] To simulate random alloys, we employ the special quasi-random structure (SQS) in 96-atom supercells. Both the lattice and internal parameters are fully relaxed.[43]

Supporting Information

Supporting Information is available from the Wiley Online Library or from the author.

Acknowledgements

A. L. and J. M. contributed equally to this work. This material is based upon work performed by the Joint Center for Artificial Photosynthesis, a DOE Energy Innovation Hub, supported through the Office of Science of the U.S. Department of Energy under Award Number DE-SC0004993. Work at the Molecular Foundry was supported by the Office of Science, Office of Basic Energy Sciences, of the U.S. Department of Energy under Contract No. DE-AC02-05CH11231. XAS data collection was carried out at the Stanford Synchrotron Radiation Lightsource (SSRL) beamline 7-3, operated by Stanford University for the U.S. DOE Office of Science, and supported by the DOE Office of Biological and Environmental Research, and by the NIH (including P41GM103393). Computations are performed using resources of the National Energy Research Scientific Computing Center (NERSC) at the LBNL that is

supported by the Office of Science of the U.S. Department of Energy under Contracts No. DE-AC02-05CH11231.

Received: ((will be filled in by the editorial staff))
Revised: ((will be filled in by the editorial staff))
Published online: ((will be filled in by the editorial staff))

References

[1] B. A. Pinaud, J.D. Benck, L.C. Seitz, A.J. Forman, Z. Chen, T.G. Deutsch, B.D. James, K.N. Baum, G.N. Baum, S. Ardo, H. Wang, E. Miller, T.F. Jaramillo *Energy Environ. Sci.* **2013**, *6*, 1983.
[2] S. Hu, C. Xiang, S. Haussener, A.D. Berger, N.S. Lewis *Energy Environ. Sci.* **2013**, *6*, 2984.
[3] H.-P. Wang, K. Sun, S. Y. Noh, A. Kargar, M.-L. Tsai, M.-Y. Huang, D. Wang, J.-H. He *Nano Lett.* **2015**, doi: 10.1021/nl5041463.
[4] L. Gao, Y. Cui, J. Wang, A. Cavalli, A. Standing, T.T.T Vu, M.A. Verheijen, J.E.M. Haverkort, E.P.A.M. Bakkers, P.H.L. Notten *Nano Lett.* **2014**, *14*, 3715.
[5] S. Hu, M. R. Shaner, J. A. Beardslee, M. Lichterman, B. S. Brunschwig, and N. S. Lewis *Science* **2014**, *344*, 1005.
[6] J. Yang, K. Walczak, E. Anzenberg, F. M. Toma, G. Yuan, J. Beeman, A.Schwartzberg, Y. Lin, M. Hettick, A. Javey, J. W. Ager, J. Yano, H. Frei, I. D. Sharp *J. Am. Chem. Soc.* **2014**, *136*, 6191.
[7] B. Mei, A. A. Permyakova, R. Frydendal, D. Bae, T. Pedersen, P. Malacrida, O. Hansen, I. E. L. Stephens, P. C. K. Vesborg, B. Seger, I. Chorkendorff *J. Phys. Chem. Lett.* **2014**, *5*, 3456.
[8] K. Sun, F. H. Saadi, M. F. Lichterman, W. G. Hale, H.-P. Wange, X. Zhou, N. T. Plymale, S. T. Omelchenko, Jr-H. He, K. M. Papadantonakis, B. S. Brunschwig, N. S. Lewis *PNAS* **2015**, *112*, 3612.
[9] K. Sivula *J. Phys. Chem. Lett.* **2013**, *4*, 1624.
[10] T.W. Kim, K.-S. Choi *Science* 2014, **343**, 2014.
[11] Y. Park, K.J. McDonald, K.-S. Choi *Chem. Rev.* **2013**, *42*, 2321.
[12] F.F. Abdi, L. Han, A.H. Smets, M. Zeman, B. Dam, R. van de Krol *Nature Comm.* **2013**, *4*, 2195.
[13] L. Chen, F.M. Toma, J.K. Cooper, A. Lyon, Y. Lin, I.D. Sharp, J.W. Ager *Chem.Sus.Chem.* **2015**, *8*, 1066.
[14] C. Jiang, R. Wang, B.A. Parkinson *ACS Combinatorial Sci.* **2013**, *15*, 639.
[15] J.K. Cooper, S. Gul, F.M. Toma, L. Chen, P.-A. Glans, J. Guo, J.W. Ager, J. Yano, I.D. Sharp *Chem. Mater.* **2014**, *26*, 5365.
[16] J. Ma, L.-W. Wang *Appl. Phys. Lett.* **2014**, *105*, 172102.
[17] H. Liu, R. Nakamura, Y. Nakato *Chem.Phys.Chem.* **2005**, *6*, 2499.
[18] D. Kang, Y. Park, J.C. Hill, K.-S. Choi *J. Phys. Chem. Lett.* **2014**, *5*, 2994.
[19] J.A. Seabold, N.R. Neale *Chem. Mater.* **2015**, *27*, 1005;
[20] F. Amano, A. Yamakata, K. Nogami, M. Osawa, B. Ohtani *J. Phys. Chem. C* **2011**, *115*, 16598.
[21] I.-S. Cho, C.H. Kwak, D.W. Kim, S. Lee, K.S. Hong *J. Phys. Chem. C* **2009**, *113*, 10647;
[22] J. Ye, Z. Zou, M. Oshikiri, A. Matsushita, M. Shimoda, M. Imai, T. Shishido *Chem. Phys. Lett.* **2002**, *356*, 221.
[23] Q. Yan, G. Li, P.F. Newhouse, J. Yu, K.A. Persson, J.M. Gregoire, J.B. Neaton *Adv. Ener. Mater.* **2015**, doi: 10.1002/aenm.201401840.

[24] S. Hu, C. Xiang, S. Haussener, A. D. Berger, N. S. Lewis *Energy Environ. Sci.* **2013**, *6*, 2984.
[25] *Handbook of Chemistry and Physics*, 95th Edition (Ed.: William M. Haynes) CRC, Boca Raton, Fla, **2014.**
[26] H. Zhang, J.S. Son, J. Jang, J.S. Lee, W.L. Ong, J.A. Malen, D.V. Talapin *ACS Nano* **2013**, *7*, 10296.
[27] J. K. Cooper, S. Gul, F. M. Toma, L. Chen, Y.-S. Liu, J. Guo, J. W. Ager, J. Yano, I. D. Sharp *J. Phys. Chem. C* **2015**, *119*, 2969.
[28] I. Vurgaftman, J. R. Meyer *App. Phys. Review* **2001**, *89*, 5815.
[29] S.-H. Wie, A. Zunger *Phys. Rev. Lett.* **1996**, *76*, 664.
[30] S.G. Kwon, T, Hyeon *Accounts of Chemical Research* **2008**, *41*, 1696.
[31] M. R. Buck, R. E. Schaak *Angew. Chemie. Int. Ed.* **2013**, *52*, 2.
[32] C. Kim, P. J. Phillips, L. Xu, A. Dong, R. Buonsanti, R. F. Klie, and J. Cabana *Chem. Mater.* **2015**, *27*, 394.
[33] S.D. Lounis, E. L. Runnerstrom, A. Llordés, and D. J. Milliron *J. Phys. Chem. Lett.* ***2014***, *5*, 1564.
[34] A. Getsoian, Z. Zhai, A.T. Bell *J. Am. Chem. Soc.* **2014**, *136*, 13684.
[35] I. Bertos, R. Jimenez, D. Perez-Mezcua, N. Salzar, J. Ricote, M. L. Calzada *Adv. Mater.* **2015**, *27*, 2608.
[36] Y. Wu, Lazic, P.; Hautier, G.; Persson, K.; Ceder G. *Energy Environ. Sci.* **2013**, *6*, 157.
[37] R. Gautier, X. Zhang, L. Hu; L. Yu, Y. Lin, T.O.L. Sunde, D. Chon, K.R. Poeppelmeier, A. Zunger *Nature Chem.* **2015**, *7*, 308.
[38] A.Walsh Nature Chem. **2015**, *7*, 274.
[39] W. Kohn, L. J. Sham *Phys. Rev.* **1965**, 140, A1133.
[40] J. P. Perdew, K. Burke, M. Ernzerhof *Phys. Rev. Lett.* **1996**, *77*, 3865.
[41] G. Kresse, J. Furthmuller *Comput. Mater. Sci.* **1996**, *6*, 15.
[42] G. Kresse, D. Joubert *Phys. Rev. B* **1999**, *59*, 1758.
[43] A. Zunger, S.-H. Wei, L. Ferreira, J. Bernard *Phys. Rev. Lett.* **1990**, 65, 353.

Scheme 1. Schematic representation for the conversion of $Bi_{1-x}Sb_x$ NC seeds to Sb-$BiVO_4$ films.

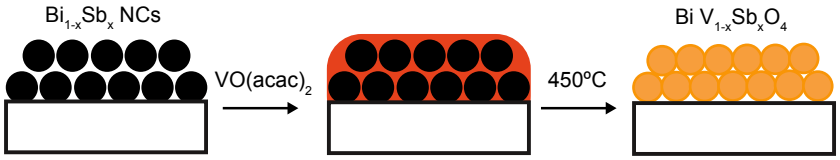

Figure 1. XRD patterns of Sb-$BiVO_4$ with different atomic percentages of Sb, as measured by ICP-OES. Monoclinic $BiVO_4$ (PDF #00-065-6028), tetragonal $SbVO_4$ (PDF #00-016-0600) and stibivanite Sb_2VO_5 (PDF #00-033-0122) reference patterns are reported.

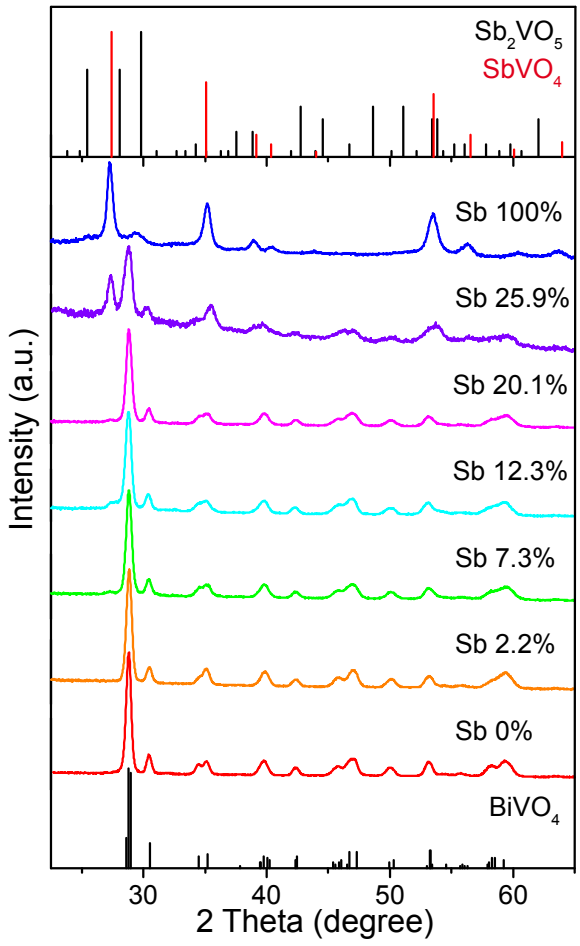

Figure 2. A) XPS spectra of Sb-$BiVO_4$ with different Sb content. The dashed black lines and continue black lines in the graphs show the O1s and Sb 3d peaks fit respectively. The Sb content increases from bottom to top. B) XANES spectra of Sb-$BiVO_4$ compared with Sb_2O_3 and Sb_2O_5 standards. C) EXAFS of the Sb-$BiVO_4$ with Sb 20.1% (magenta curve) and the first-shell fit (black curve) assuming Sb occupies the V site.

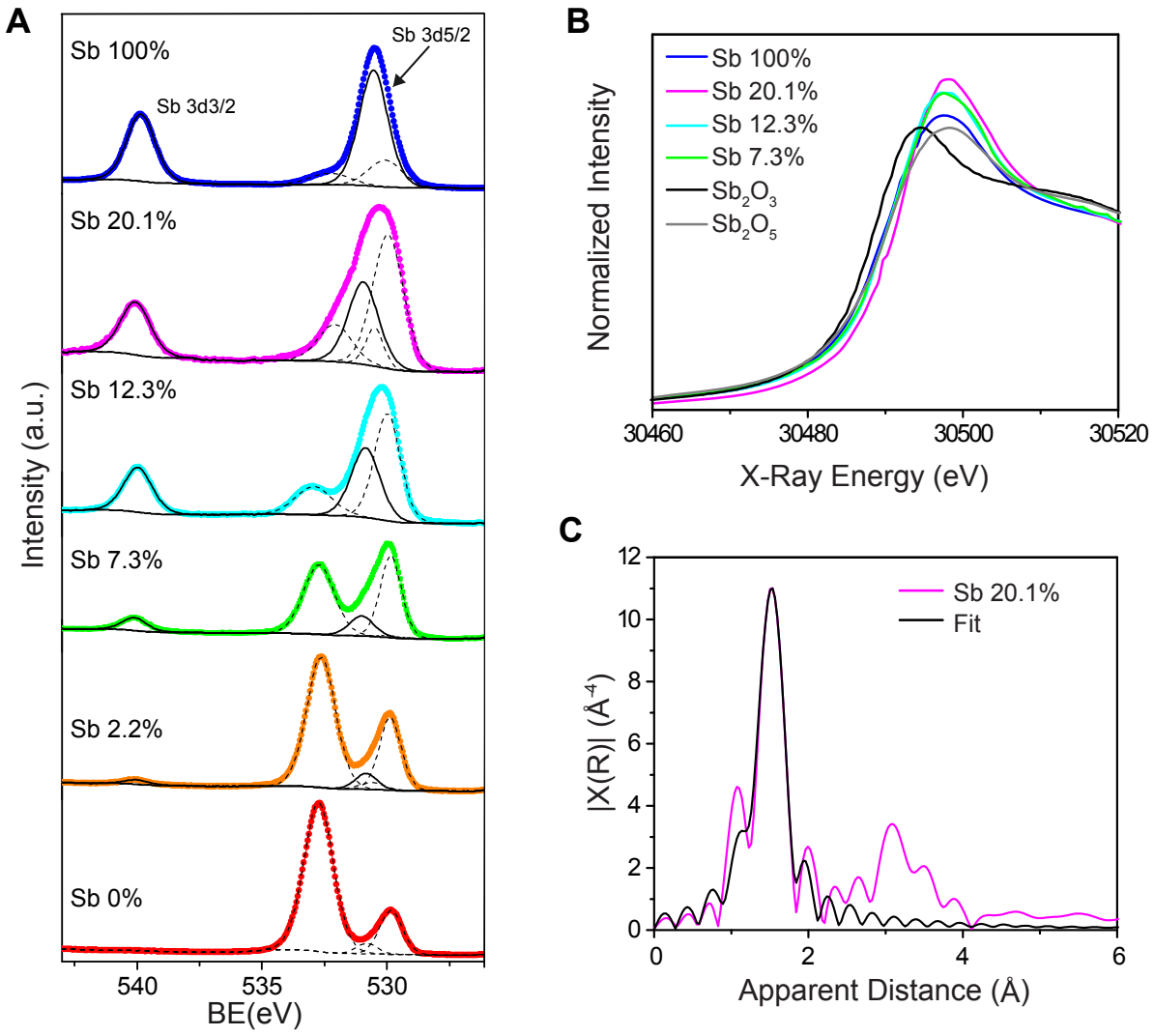

Figure 3. A) Diffuse reflectance spectra of Sb-$BiVO_4$ with different Sb content collected using an integrating sphere as a function of wavelength. B) and C) Tauc plots for the same samples corresponding to direct and indirect transitions, respectively, along with linear fits (dashed lines) of the absorption edges. The black points indicate the corresponding band gaps.

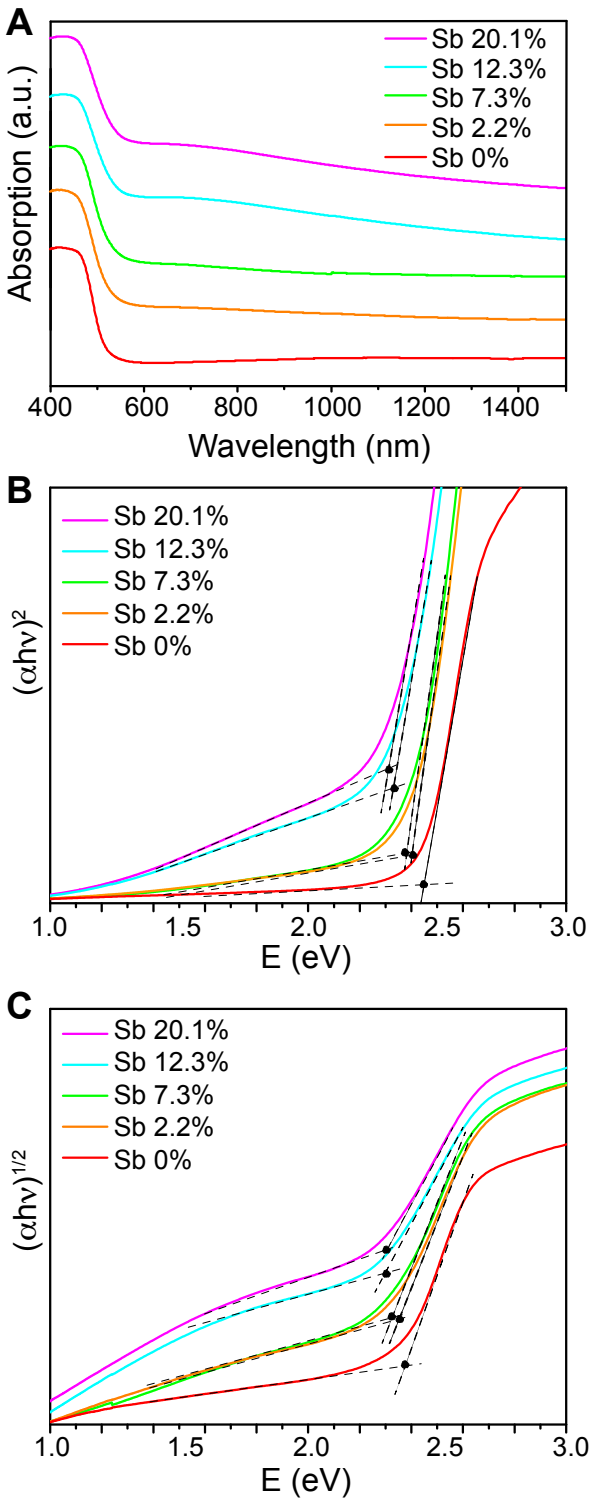

Figure 4. A) Dependence of the calculated band gap of the $BiV_{1-x}Sb_xO_4$ alloys on the composition parameter, *x*. B) The CBM charge densities (yellow isosurfaces) in $BiV_{1-x}Sb_xO_4$ alloys with (a) x = 0.0625, (b) x = 0.25, (c) x = 0.5, and (d) x = 0.75.

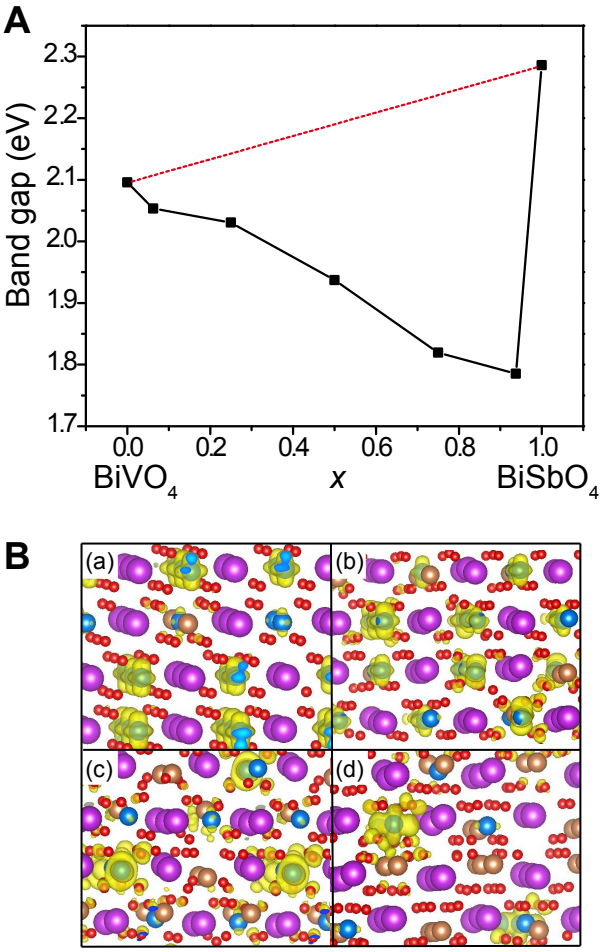

Figure 5. A) Schematic representation of the conversion of In_2O_3, Bi, Sn, and Cu NCs seeds into different ternary oxides and B) corresponding XRD patterns. Reference patterns of orthorombic $InVO_4$ (PDF# 04-008-7237), orthorombic Bi_2WO_6 (PDF# 00-039-0256), orthorombic $SnWO_4$ (PDF# 00-029-1354) and triclinic $CuWO_4$ (PDF# 01-073-1823) are reported in each graph.

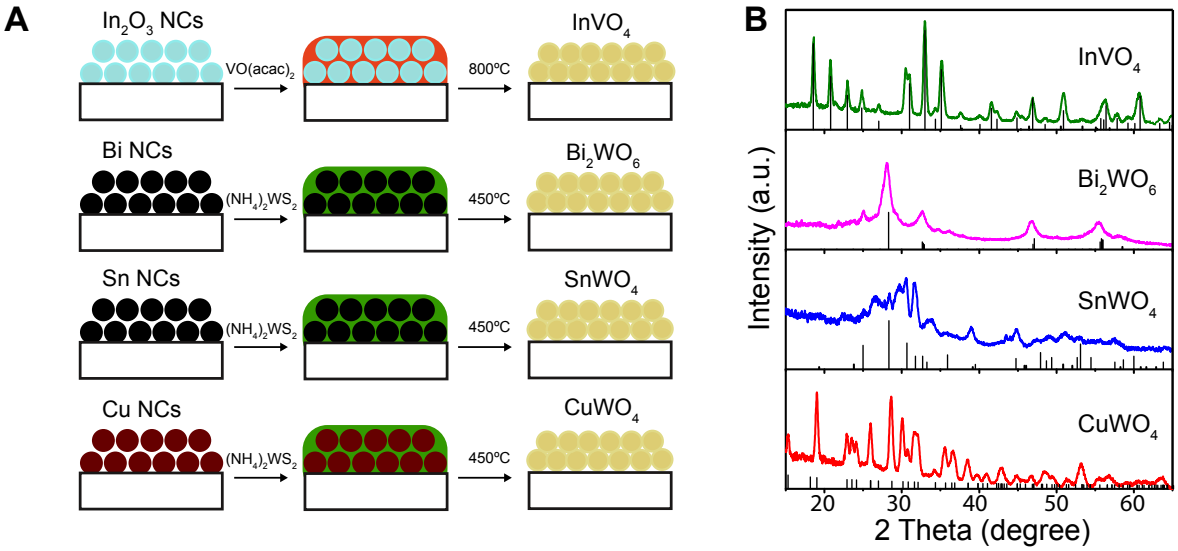

The challenge of fine compositional tuning and microstructure control in complex oxides is overcome by developing a general two-step synthetic approach. Antimony-alloyed bismuth vanadate, herein identified as a novel light absorber for solar fuel applications, is prepared in a wide compositional range. The band gap of this quaternary oxide linearly decreases with the Sb content, in agreement with first-principles calculations.

Keyword

A. Loiudice, J. Ma, W. S. Drisdell, T. M. Mattox, T. Thao, J. K. Cooper, C. Giannini, J. Yano, I. D. Sharp, L.-W. Wang, R. Buonsanti*

Band gap Tunability in Sb-alloyed $BiVO_4$ Quaternary Oxides as Visible-Light Absorbers for Solar Fuel Applications

ToC figure